# High-resolution photoabsorption near the sulfur $L_{2,3}$ thresholds: $H_2S$ and $D_2S$

E. Hudson

*Department of Chemistry, University of California and Chemical Sciences Division, MS 2-300, Lawrence Berkeley Laboratory, 1 Cyclotron Road, Berkeley, California 94720*

D. A. Shirley

*Departments of Chemistry and Physics, Pennsylvania State University, University Park, Pennsylvania 16802*

M. Domke, G. Remmers, and G. Kaindl

*Institut für Experimentalphysik, Freie Universität Berlin, Arnimallee 14, W-1000 Berlin 33, Germany*

(Received 21 June 1993)

The x-ray-absorption near-edge structure of gas-phase $H_2S$, hydrogen sulfide, and $D_2S$, deuterium sulfide, at the sulfur $L_{2,3}$ ionization thresholds has been measured using synchrotron radiation with high-energy resolution from the SX700/II soft-x-ray monochromator at the Berliner Elektronenspeicherring-Gessellschaft für Synchrotronstrahlung m.b.H. Previously unobserved fine structure is resolved. The spectra of both molecules are characterized by multielectron excitations 8–14 eV above the $L_2$ threshold energy, broad valence-shell absorption features 5–8 eV below the $L_2$ edge, and many narrower Rydberg excitations 0–5 eV below the $L_2$ edge. Comparison of the $H_2S$ and $D_2S$ spectra allows the identification of transitions which include vibrational excitation, due to the isotopic dependence of vibrational energies. For the $(2p)^{-1}$ core-excited Rydberg states, a least-squares analysis was employed, which deconvoluted the core-level and excited-orbital splittings. Results show that the twofold degeneracy of the sulfur $2p_{3/2}$ core level is removed by the molecular field, with a resulting splitting of 115 meV for the higher-energy core-excited Rydberg states. The energies of the higher Rydberg states were well described by the Rydberg formula with the quantum defects $\delta_p = 1.63$ and $\delta_d = 0.32$. Fine structure was resolved in the transitions to the dissociative $(2p)^{-1}$ core-excited valence-shell states. The regular spacing and isotopic dependence of this structure clearly identifies it as a vibrational progression.

PACS number(s): 33.20.Rm, 33.70.−w, 33.80.Eh, 33.80.Rv

## I. INTRODUCTION

The core levels of an atom exhibit a small but, in many cases, measurable sensitivity to chemical environment [1]. Besides its significance to a comprehensive understanding of molecular and condensed-phase electronic structure, this dependence is important in several widely used spectroscopic techniques, e.g., Auger-electron spectroscopy (AES) and x-ray photoelectron spectroscopy (XPS). In this paper, analysis of high-resolution molecular x-ray-absorption near-edge-structure (XANES) spectra allows the measurement of the molecular-field splitting of a core level. This result demonstrates the potential of high-resolution core-level spectroscopies for the study of atomic-core structure in different chemical surroundings.

The measurement of soft-x-ray photoabsorption spectra of atoms and molecules has been facilitated over the past few years by developments in monochromators at synchrotron radiation facilities [2–5]. As a result, core-level photoabsorption features in a variety of systems have been studied with improved sensitivity and energy resolution. Concurrent advances in data analysis allowed the extraction of detailed information about the electronic, vibrational, and geometric structure of core-excited states in $N_2$ [6], CO [7], $C_2H_4$ [8], $H_2CO$ [9], $SF_6$ [10], and other molecules [11]. This paper extends this work by presenting high-resolution XANES measurements of hy-

drogen sulfide, $H_2S$, and its fully deuterated analog, $D_2S$, near the sulfur $L_{2,3}$ ionization thresholds. A detailed understanding of the spectra is obtained by applying alternative approaches in data analysis.

Previous photoabsorption measurements near the $L_{2,3}$ thresholds of $H_2S$, as well as other third-row hydrides, yielded complicated spectra with many overlapping sharp lines preceded at lower energy by a few broader features [5,12]. The latter features were assigned to one-electron transitions of a sulfur $2p$ electron into the two lowest unoccupied molecular orbitals [13,14]. Following the terminology used at lower photon energies [15], these core-excited states are referred to here as "valence-shell states." The sharper peaks at higher energies were assigned to transitions into several series of atomiclike Rydberg orbitals leading up to the ionization thresholds. These "Rydberg states," in particular, were difficult to assign fully due to limited resolution and statistics. In the present work, these limitations were overcome, and the assignment is now limited more by the complexity of the spectrum than by the quality of the data. The analysis presented here unambiguously assigns the higher Rydberg states converging on the sulfur $L_{2,3}$ edges. A more tentative assignment of the lower Rydberg states is also given. Most important, however, is the determination of the core hole corresponding to each feature, and thus the term value of the associated Rydberg orbital. To

accomplish this, a least-squares analysis was employed, which allowed the deconvolution of core-level and excited-orbital splittings.

The sulfur $2p$ core orbitals are split into $2p_{3/2}$ and $2p_{1/2}$ levels by spin-orbit interaction. This $\approx 1.2$ eV splitting has been measured previously by XANES, AES, and XPS [12,16–18]. The atomic $2p_{3/2}$ level is doubly degenerate, but in the $C_{2v}$ symmetry of the $H_2S$ molecule, this degeneracy may be removed by the anisotropic molecular field. A recent comparison of high-resolution XPS and AES suggested that this splitting is $\approx 106$ meV in core-ionized $H_2S^+$ [16]. In this paper, the least-squares analysis confirms the molecular-field splitting of the sulfur $2p_{3/2}$ level, and determines it to be 115 meV for the higher Rydberg states. Because the total observed linewidths of the Rydberg peaks are $\approx 70$ meV in this experiment, this splitting has a notable effect upon the spectrum.

Photoabsorption [19] and especially photoelectron spectroscopy [20] have been used to measure molecular-field splittings in the $3d$ and $4d$ levels of a number of elements. The molecular-field splitting of the $2p_{3/2}$ core level has been predicted for the XANES spectra of Cl and P compounds, and has possibly been resolved for $PH_3$ [21,22]. The pronounced multiplet splitting of the (S $2p_{3/2,1/2})^{-1}$ $3b_1$ resonances in $SO_2$ indicates a sizable anisotropic influence on the sulfur $2p$ levels in these electronic states, but these effects are not seen for the higher-energy (S $2p)^{-1}$ Rydberg resonances in $SO_2$ [23]. The present work clearly resolves the $2p_{3/2}$ core-level splitting in the XANES spectrum of $H_2S$. With an ionization energy of $\approx 170$ eV, this is the deepest core level for which this splitting has been measured.

XANES spectra of $D_2S$ were measured for the first time to aid in the assignment of the spectra. Transitions which include the excitation of vibrational modes are identified by a shift in energy upon deuteration of the molecule, because of the isotopic dependence of vibrational frequencies. Isotopic differences appear mainly in the region of the spectra between the valence-shell and upper Rydberg excitations. Spectral features in this region are characterized by narrow linewidths, like the Rydberg states at higher energies, and by extensive vibrational progressions, as observed for the valence-shell states at lower energies. For these reasons, and others, these features are assigned to transitions to "mixed orbitals," intermediate in spatial distribution and in energy between the valence and Rydberg orbitals [15].

Creation of a $2p$ core hole may affect the bonding of the molecule, but that influence should be nearly the same for any of the three nondegenerate $2p$ core holes (i.e., the single $2p_{1/2}$ hole and the two molecular-field-split $2p_{3/2}$ holes). Therefore the three nondegenerate excited states resulting from promotion of a $2p$ electron into a particular final-state orbital should have essentially the same vibrational structure. The associated spectrum will contain a partially overlapping set of three vibrational progressions, offset in energy from each other, but otherwise identical. In principle, deconvoluting the contribution of the core-level splitting to the spectrum will reveal

the vibrational spacings corresponding to the excitation of each individual final-state orbital. In fact, because of overlapping vibrational progressions the resulting information is still too complicated for a definitive assignment and/or a Franck-Condon analysis.

Fine structure with an isotopic dependence is also observed in the broad, lower-energy features of the spectra. This regularly spaced structure is only barely resolved, due to the large natural linewidths of the valence-shell excitations. Vibrational excitation is expected for these transitions into unoccupied molecular orbitals, because at least one of the orbitals accessed is strongly antibonding [24,13]. Putting an electron into an antibonding orbital tends to lengthen bonds and thus induce vibrational excitations, unless there are strong compensating effects from the creation of the core hole. Recent studies showed that rapid dissociation is an important decay process for these core-excited valence-shell states [25–27]. Interpretation of the vibrational structure is complicated by this dissociation and by the possibility of vibronic interaction between the electronic states in this energy range.

## II. EXPERIMENT

Photoabsorption spectra were recorded by passing soft x rays through a gas cell and measuring the total ion current produced as a function of photon energy. The Freie Universität Berlin SX-700/II plane grating monochromator [2,3] was used to select a very narrow bandwidth of soft-x-ray synchrotron radiation from the Berliner Elektronenspeicherring für Synchrotronstrahlung (BESSY). The 2442-line/mm grating, used in the first order of diffraction, produced the optimum combination of
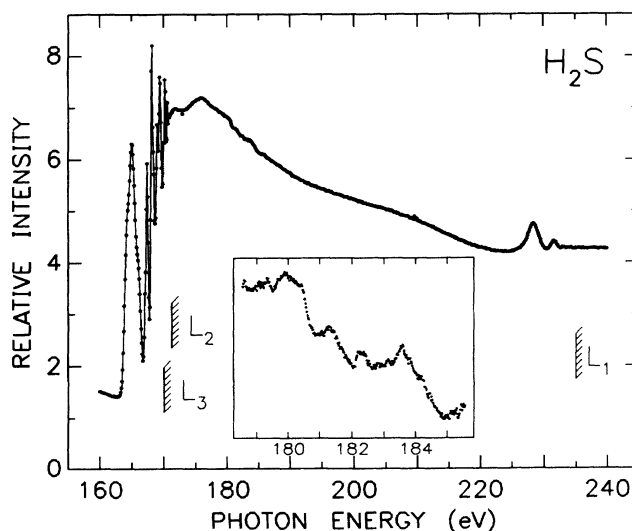


FIG. 1. Overview of the photoabsorption spectrum of $H_2S$ near the sulfur $L$ edges. The positions of the ionization thresholds determined from analysis of the spectra are also shown. The small molecular-field splitting of the $L_3$ edge is not visible with this energy scale. The inset shows a higher-resolution spectrum in the 178.56–185.56-eV range, with the energy scale expanded by a factor of 5. The absorption features in this range are attributed to multielectron excitations.

flux and energy resolution. For the measurements near the sulfur $L_{2,3}$ edges, the resolution was $\approx 30$ meV [Gaussian full width at half maximum (FWHM)]. The absolute energy scale for the $H_2S$ spectra was established by comparison to the energy of the $0 \rightarrow 0$ vibrational transition of the $N_2$ $(1s)^{-1}$ $\pi^*$ resonance at 400.88 eV [28]. The estimated uncertainty of this calibration is 0.01 eV at 167 eV. The energy scale for the $D_2S$ spectra was obtained by assuming the $(2p_{1/2})^{-1}$ $5d$ Rydberg state at 170.94 eV has the same energy in both $H_2S$ and $D_2S$. The estimated uncertainty of the relative energy scale over a 4-eV-wide range is 12 meV for $H_2S$ and 5 meV for $D_2S$, with smaller errors for narrower energy ranges. The gas

cell contained $H_2S$ (Messer Griesheim, 99.3%) or $D_2S$ (CIL, 98%) at a typical pressure of 0.10 mbar. A 1000-Å carbon window separated the gas cell from the ultrahigh vacuum of the monochromator.

## III. RESULTS

Figure 1 shows an overview of the $H_2S$ photoabsorption spectrum in the 160–240-eV photon energy range. Intense resonances are apparent below the sulfur $L_1$ ionization threshold at $\approx 235$ eV and the sulfur $L_{2,3}$ thresholds at $\approx 171$ eV. The region below the $L_{2,3}$ thresholds contains an extensive series of peaks, shown in greater detail in Figs. 2 and 3. The inset of Fig. 1 shows a higher-
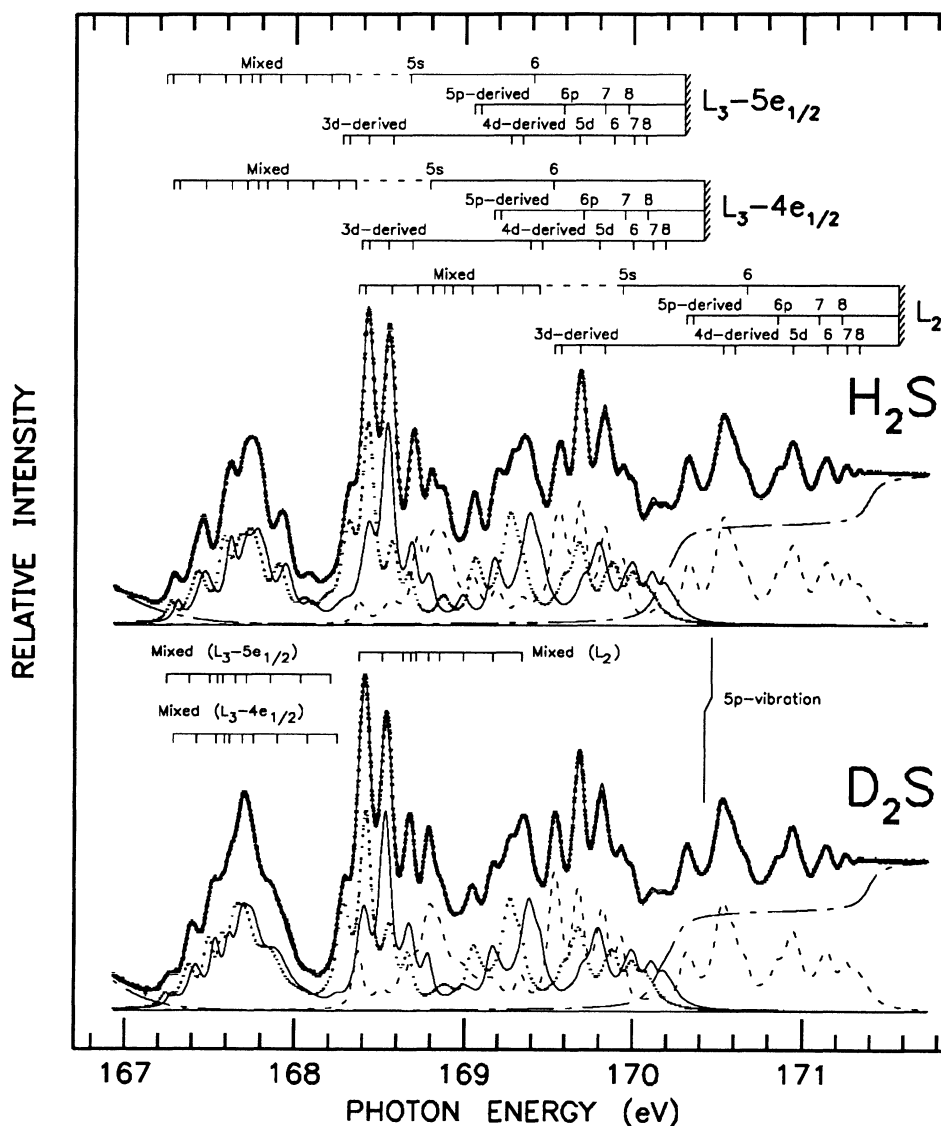


FIG. 2. High-resolution photoabsorption spectra of $H_2S$ and $D_2S$ in the mixed and Rydberg region of the sulfur $L_{2,3}$ edges. Rydberg assignments applying to both spectra are shown, identifying $s$, $p$, and $d$ series converging on each of the three ionization thresholds. Note that the $s$ assignments are less certain than the others. For the mixed states, different assignments are shown for the two spectra, because of the large isotopic differences for these states. The isotopic shift of the $(2p_{1/2})^{-1}$ $5p$ vibrational sideband, as determined from the fit, is indicated by the vertical line. Data points are plotted as circles. Results of a least-squares analysis are plotted as solid lines. Contributing subspectra plotted underneath, with dashed lines showing features attributed to $2p_{1/2}$ core-hole states, solid lines showing features attributed to $2p_{3/2}$-$4e_{1/2}$ core-hole states, and dotted lines showing features attributed to $2p_{1/2}$-$5e_{1/2}$ core-hole states. See Sec. IV B 3 a for further details.
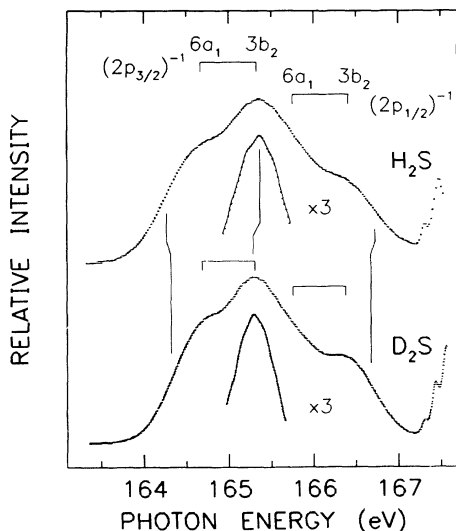
FIG. 3. High-resolution photoabsorption spectra of $H_2S$ and $D_2S$ in the region of valence-shell excitations below the sulfur $L_{2,3}$ edges. The vertical lines indicate isotopic shifts in some features of the peak. Portions of the data are also shown with the vertical scale expanded, to display the weakly resolved fine structure. The results of a least-squares analysis are plotted as solid lines with the expanded data. For $D_2S$, the fit line is not visible, due to the large point density and the high quality of the fit.

resolution spectrum of the weak features in the range 178.56–185.56 eV. Note that the energy scale of the inset is five times that of the main spectrum. Similar structure is also observed in the corresponding spectrum of $D_2S$. These peaks are attributed to multielectron excitations.

Figure 2 shows the high-resolution spectra of $H_2S$ and $D_2S$ in the range $\approx 167-172$ eV. For both spectra, the complicated pattern of absorption features is assigned to one-electron excitations from the sulfur $2p$ core levels to several series of intermediate and Rydberg orbitals. These orbitals may be split into several components by the anisotropic molecular field. Additionally, each final-state orbital is accessed by transitions from the three nondegenerate sulfur $2p$ core levels. The large number of dipole-allowed transitions is further increased by the possibility of vibrational excitations accompanying the electronic excitation. Differences between the two spectra are most prominent in Fig. 2 for the lower-energy range $\approx 167-168$ eV, i.e., the region of transitions to mixed states. These differences are expected in the vibrational sidebands of electronic transitions due to the strong isotopic dependence of vibrational frequencies.

The lowest-energy absorption features of Fig. 1 are shown with much higher energy resolution in Fig. 3, along with the corresponding spectrum of $D_2S$. These peaks are assigned to one-electron transitions from the sulfur $2p$ core level to the unoccupied $6a_1$ and $3b_2$ molecular orbitals. Both of these transitions are split by the nondegeneracy of the sulfur $2p$ core electrons. The weak fine structure apparent in both spectra is also shown in Fig. 3 with an expanded intensity scale. These regularly

spaced features, seen here for the first time, are attributed to the excitation of vibrations in the final state. Small isotopic shifts in the overall peak width and position were also observed, as indicated by the vertical lines.

## IV. ANALYSIS AND DISCUSSION

### A. Sulfur $L_{2,3}$ edges:
### Nondegeneracy of the sulfur $2p$ core level

$2p$ core electrons exhibit a well-known spin-orbit splitting, indicated by the $L_{2,3}$ notation for the two distinct $2p$ ionization thresholds. This effect occurs even in free atoms, e.g., the splitting is clearly observed in the gas-phase argon $L_{2,3}$ XANES spectrum [2,29]. In the molecular case, however, the atomic spherical symmetry is removed. Specifically, the $H_2S$ molecule has $C_{2v}$ symmetry, which splits the sulfur $2p$ core level into *three* energy levels. In the atomic case, the spin-orbit interaction splits the $2p$ core level into the $2p_{1/2}$ and the twofold degenerate $2p_{3/2}$ levels. When the influence of the anisotropic molecular field of $H_2S$ is also considered, the degeneracy of the sulfur $2p_{3/2}$ level is removed. The two resulting levels may be designated $4e_{1/2}$ and $5e_{1/2}$ in the extended point group which applies to $C_{2v}$ symmetry. In this paper these core levels are labeled $2p_{3/2}\text{-}4e_{1/2}$ and $2p_{3/2}\text{-}5e_{1/2}$, and the corresponding ionization thresholds are $L_3\text{-}4e_{1/2}$ and $L_3\text{-}5e_{1/2}$, where the latter core level is the shallower of the two and thus the latter threshold has the lower energy of the two. The abbreviated label $2p_{3/2}$ refers to both levels. The deepest $2p$ level is still best described as $2p_{1/2}$ because the molecular-field splitting is much smaller than the spin-orbit splitting. For convenience, the difference between the energy of a $(2p_{1/2})^{-1}$ state and the average energy of the two corresponding $(2p_{3/2})^{-1}$ states will be called the mean spin-orbit splitting, although this quantity may in fact be influenced by the molecular field and by the interaction of the excited electron with the core hole.

It is important to recognize the distinction between the energy splittings of the sulfur $2p$ core levels in the core-excited ion, as measured by XPS, and the splittings which are observed in photoabsorption. In XPS, in the high kinetic-energy limit, the splittings observed are those of the core levels in the electronically relaxed core-excited ion. In the near-edge photoabsorption measurements, however, one must also account for the influence of the excited electron. As in the atomic case, the exchange interaction between the excited electron and the core electrons may modify the observed splittings. However, there are now three configurations of the molecular core electrons, corresponding to the three possible core holes, rather than two. Thus there are two energy splittings which may be modified, rather than one. In $H_2S$ it is possible for the direct Coulombic interaction between the excited electron and the $2p$ electrons to influence the observed splittings. This is possible because, in contrast to the atomic case, the $2p$ electrons occupy nonidentical spatial orbitals and thus the direct Coulombic repulsion between the excited electron and the three possible configurations of core electrons may vary. Both the ex-

change and direct interactions will be largest for states in which the excited electron has strong spatial overlap with the core. Dipole-allowed transitions to such states should be intense because of this overlap.

## B. Sulfur $L_{2,3}$ edges: Rydberg and mixed excitations

### 1. General considerations

The geometric [30] and electronic structures of ground-state $H_2S$ and $D_2S$ are very similar. Therefore differences between the photoexcitation spectra of the two molecules are expected primarily as a result of the large differences in vibrational frequencies between the two molecules in their final excited states. Figure 2 shows high-resolution spectra of $H_2S$ and $D_2S$ in the region of the intermediate and Rydberg excitations. Upon comparison of the spectra, it is apparent that isotopic differences lie mainly in the lowest third of the energy range shown. Therefore some electronic transitions in this lower range must include vibrational excitations. Vibrational sidebands are often observed for transitions to core-excited molecular Rydberg states [6–11]. However, the large isotopic differences seen here indicate more extensive vibrational excitations than are normally seen for Rydberg states. The excited electron may therefore be better described as possessing both Rydberg-orbital and molecular-orbital character. These states are referred to here as "mixed" or intermediate states, as mentioned in the Introduction.

Further comparison shows that the $H_2S$ and $D_2S$ spectra in Fig. 2 are nearly identical in the upper third of the energy range. An immediate conclusion is that above $\approx 169$ eV the spectra contain, at most, minor contributions from vibrational sidebands. Thus the rich fine structure of the upper region arises only from electronic excitations, *without* vibrational excitation. By comparison, the corresponding region of the $L_{2,3}$ absorption spectrum for the isoelectronic rare-gas atom, argon [2,29], is much less complex. One complicating factor for $H_2S$ is the molecular-field splitting of the sulfur $2p_{3/2}$ core level, as mentioned above. The influence of the $C_{2v}$-symmetry molecular field upon the Rydberg orbitals and upon the dipole-selection rules must also be considered. For the Rydberg orbitals, the molecular field can completely remove the spatial degeneracies of the $p$ and $d$-symmetry orbitals. In addition, the selection rules are relaxed in the lower symmetry, allowing more transitions than in the atomic case. A full group-theoretical treatment of electronic transitions in $H_2S$ is obtained by applying the concepts presented in Ref. [31]. The results show that ground-state transitions are dipole allowed to nine electronic final states corresponding to the $2p^{-1}$ $ns$ atomic configuration for a *single* value of $n$. Likewise, transitions are dipole allowed to 27 (45) electronic final states corresponding to the $2p^{-1}$ $np$ ($2p^{-1}$ $nd$) atomic configuration for a single value of $n$.

For the corresponding excitations in Ar, there are dipole-allowed transitions only to $2p^{-1}$ $ns$ and $2p^{-1}$ $nd$ configurations. These result in two and three triply degenerate states, respectively, totaling 15 states altogether,

for a single value of $n$. In $H_2S$, for the same shell $n$, there are dipole-allowed transitions to 81 singly degenerate states. In light of these numbers, it becomes evident that the Rydberg spectra observed for $H_2S$ and $D_2S$ are in fact much simpler than they would be if all possible states were resolved. This is not surprising, because the Rydberg orbitals, which extend far away from the molecule, are only affected by a weak molecular field. The higher Rydberg orbitals, in particular, behave much like atomic orbitals and the corresponding transitions are readily assigned. And even purely atomic splittings might not be resolved. For example, in the Ar $L_{2,3}$ spectrum, the spin-orbit splitting of the $nd$ Rydberg orbitals is too small to be observed [29].

Peak energies, intensities, and linewidths were extracted from the data in Fig. 2 using a least-squares fitting routine. Voigt functions modeled the line shapes of the absorption peaks and Gaussian-broadened arctangent functions modeled the edge jumps. To account for the "pileup" of unresolved transitions just below the ionization thresholds [32], each edge jump was shifted $-172$ meV relative to the threshold energies determined from the Rydberg analysis. Results of the least-squares analysis are presented in Tables I and II and are plotted with the data in Fig. 2. Further details of the data analysis are given below, as necessary.

### 2. Upper range: Rydberg states

The region of the Rydberg spectrum above 170.4 eV is the simplest to interpret because it lies above the $L_3$-$4e_{1/2}$ and $L_3$-$5e_{1/2}$ ionization thresholds. All the peaks observed must therefore correspond to excitations from the sulfur $2p_{1/2}$ core level. For the region above 170.8 eV, the interpretation is further facilitated by assuming that only atomic splittings apply, so that $s$-, $p$-, and $d$-symmetry Rydberg series may be identified. Note that the reduced symmetry of $H_2S$ relaxes the atomic dipole-selection rule which forbids $2p$ to $np$ transitions. Above 170.8 eV, the least-squares analysis of the $H_2S$ and $D_2S$ spectra assumed that transition energies were given by the Rydberg formula. Excellent fits were obtained using the quantum defects $\delta_p = 1.63$ and $\delta_d = 0.32$, with the sulfur $L_2$ ionization threshold at 171.564 eV. The assignment of these quantum defects to the $p$ and $d$ Rydberg series is supported below in Sec. IV B 4 b, in the light of a comparison to the corresponding quantum defects for some isoelectronic systems.

The region between 170.3 and 170.8 eV is somewhat more complicated. Two prominent peaks are observed at 170.315 and 170.534 eV, near the energies predicted by the Rydberg formula for the (S $2p_{1/2}$)$^{-1}$ $5p$ and (S $2p_{1/2}$)$^{-1}$ $4d$ states, respectively, but both show high-energy shoulders. The spectra of $H_2S$ and $D_2S$ are very similar in this region, indicating that vibrational sidebands are not present, beyond the exception described below. The energies discussed here are for $H_2S$, but the corresponding values for $D_2S$ are nearly the same (see Table I). The most prominent peak associated with the (S $2p_{1/2}$)$^{-1}$ $4d$ state has a transition energy 26 meV less than the value predicted by $\delta_d$. Two shoulders lie 70 and

136 meV above this prominent peak. The first shoulder is assigned, like the main peak, to the (S $2p_{1/2})^{-1}$ $4d$ state; i.e., there is a 70-meV splitting observed in the transition to the $4d$ orbital. As discussed above, the influence of the molecular field can remove the spatial degeneracy of the $d$ orbital and relax angular-momentum restrictions on transitions. Many transitions may be observed which are derived from a single atomic transition, and the assignments given in Table I stress that correspondence wherever possible. The second shoulder is tentatively assigned to a transition to the $6s$ Rydberg orbital, with a resulting quantum defect of $\delta_s = 2.10$. This feature could alternatively be attributed to yet another component of the (S $2p_{1/2})^{-1}$ $4d$ state. The prominent peak and large shoulder associated with the (S $2p_{1/2})^{-1}$ $5p$ state have transition energies 49 and 11 meV less than the value predicted by $\delta_p$. Thus the splitting of the $5p$ state is 38 meV. Note that these two features lie at low enough energies to include contributions from states with a $2p_{3/2}$-$4e_{1/2}$ core hole, but fine structure is not expected in the region immediately below an ionization threshold.

The detailed fits of the (S $2p_{1/2})^{-1}$ $5p,4d$ region showed a notable difference between the $H_2S$ and $D_2S$ spectra which is not easily detected by eye; the low-intensity feature at 170.466 eV in $H_2S$ is shifted $-43$

meV in $D_2S$ (see Table I and Fig. 2). This shoulder is assigned to a vibrational sideband of the intense $5p$-derived transition at 170.315 eV (170.309 eV) in $H_2S$ ($D_2S$). The derived vibrational spacing for the excited state is 153 meV (114 meV) for $H_2S$ ($D_2S$). These values suggest an assignment to the $v_2$ bending mode, with a ground-state spacing of 147 meV (106 meV) [33]. Other vibrational results are discussed below in Sec. IV B 6. Another low-intensity feature in this region, which lies at 170.807 eV in $H_2S$, is shifted $-16$ meV in $D_2S$. Neither the isotopic shift nor the spacing of the nearby states suggest a simple vibrational assignment for this feature. It could be attributed to a molecular-field-split component of the nearby (S $2p_{1/2})^{-1}$ $6p$ state, but that implies a larger splitting than observed for the (S $2p_{1/2})^{-1}$ $5p$ state and does not explain the isotopic energy dependence.

### 3. Lower range: Rydberg and mixed states

*a.  Approach  used  for  analysis.*  In  the  range 166.8–170.3 eV, interpretation of the $H_2S$ and $D_2S$ spectra is more difficult. An independent least-squares fit of the $\approx 65$ transitions observed in this range for the two spectra would require an adjustable energy, intensity, and linewidth for each transition. Such an analysis could pro-

TABLE I. $H_2S$ and $D_2S$ $2p$ Rydberg resonances: Assignments and fit results. The energies tabulated apply to states with the (S $2p_{1/2})^{-1}$ core vacancy. Energies for corresponding states with (S $2p_{3/2}$-$4e_{1/2})^{-1}$ and (S $2p_{3/2}$-$5e_{1/2})^{-1}$ core vacancies can be obtained by subtraction of term values from the tabulated energies of the $L_3$-$4e_{1/2}$ and $L_3$-$5e_{1/2}$ edges. The Rydberg-orbital assignments shown apply to all three possible core vacancies. The intensity ratio $X$ is a dimensionless fit parameter defined in the text.

| $H_2S$ | | | | | $D_2S$ | | |
|---|---|---|---|---|---|---|---|
| Energy (eV) | Term value (eV) | Intensity | Assignment | Intensity ratio ($X$) | Energy (eV) | Term value (eV) | Intensity |
| 169.535 | 2.029 | 422 | $3d$ derived | 0.20 | 169.527 | 2.037 | 518 |
| 169.577 | 1.987 | 589 | $3d$ derived | 1.07 | 169.557 | 2.007 | 626 |
| 169.688 | 1.876 | 1010 | $3d$ derived | 1.72 | 169.680 | 1.884 | 930 |
| 169.833 | 1.731 | 660 | $3d$ derived | 0.78 | 169.822 | 1.742 | 885 |
| 169.935 | 1.629 | 399 | $5s$ derived? | 0.70 | 169.933 | 1.631 | 391 |
| 170.134 | 1.430 | 81 | ? | 2.50 | 170.143 | 1.421 | 116 |
| 170.303 | | | $L_3$-$5e_{1/2}$ edge | | 170.303 | | |
| 170.315 | 1.249 | 298 | $5p$ derived | 1.14 | 170.309 | 1.255 | 267 |
| 170.353 | 1.211 | 192 | $5p$ derived | 0.79 | 170.351 | 1.213 | 210 |
| 170.418 | | | $L_3$-$4e_{1/2}$ edge | | 170.418 | | |
| 170.466 | 1.098 | 90 | vibration | 2.50 | 170.423 | 1.141 | 94 |
| 170.534 | 1.030 | 1175 | $4d$ derived | 1.01 | 170.532 | 1.032 | 1180 |
| 170.604 | 0.960 | 243 | $4d$ derived | 0.98 | 170.601 | 0.963 | 249 |
| 170.670 | 0.894 | 240 | $6s$? | 0.20 | 170.667 | 0.897 | 243 |
| 170.807 | 0.757 | 118 | ? | 0.76 | 170.791 | 0.773 | 118 |
| 170.851 | 0.713 | 115 | $6p$ | 0.88 | 170.851 | 0.713 | 114 |
| 170.943 | 0.621 | 1000 | $5d$ | 1.04 | 170.943 | 0.621 | 1000 |
| 171.092 | 0.472 | 46 | $7p$ | 1.00 | 171.092 | 0.472 | 41 |
| 171.142 | 0.422 | 546 | $6d$ | 1.00 | 171.142 | 0.422 | 549 |
| 171.228 | 0.336 | 10 | $8p$ | 1.00 | 171.228 | 0.336 | 11 |
| 171.259 | 0.305 | 281 | $7d$ | 1.00 | 171.259 | 0.305 | 283 |
| 171.333 | 0.231 | 129 | $8d$ | 1.00 | 171.333 | 0.231 | 127 |
| 171.564 | 0 | | $L_2$ edge | | 171.564 | 0 | |

TABLE II. $H_2S$ and $D_2S$ $2p$-mixed resonances: Fit results and vibrational assignments. The energies tabulated apply to states with the $(S\ 2p_{1/2})^{-1}$ core vacancy. Energies for corresponding states with $(S\ 2p_{3/2}\text{-}4e_{1/2})^{-1}$ and $(S\ 2p_{3/2}\text{-}5e_{1/2})^{-1}$ core vacancies can be obtained by subtraction of term values from 170.471 and 170.432 eV, respectively. The intensity ratio $X$ is a dimensionless fit parameter defined in the text. The assignments shown apply to all three possible core vacancies. Tentative assignments of vibrational progressions are identified by $A1$, $A2$, etc. The energy spacing between successive states of a progression, e.g., $E_{A2}-E_{A1}$, is also listed.

| Energy (eV) | Term value (eV) | Intensity | Intensity ratio ($X$) | Vibrational assignment | Vibrational spacing (meV) |
|---|---|---|---|---|---|
| | | | $H_2S$ | | |
| 168.371 | 3.193 | 91 | 0.20 | | |
| 168.407 | 3.157 | 33 | 2.04 | $A1$ | |
| 168.564 | 3.000 | 246 | 2.50 | $A2$ | 157 |
| 168.716 | 2.848 | 505 | 0.96 | $A3$ | 152 |
| 168.806 | 2.758 | 629 | 0.88 | | |
| 168.872 | 2.692 | 524 | 1.04 | $A4$ | 156 |
| 168.923 | 2.641 | 204 | 1.38 | | |
| 169.040 | 2.524 | 457 | 1.18 | $A5$ | 164 |
| 169.190 | 2.374 | 260 | 0.52 | $A6$ | 150 |
| 169.340 | 2.224 | 167 | 0.20 | $A7$ | 150 |
| 169.443 | 2.121 | 122 | 1.23 | | |
| | | | $D_2S$ | | |
| 168.377 | 3.187 | 364 | 0.20 | | |
| 168.514 | 3.050 | 157 | 2.49 | | |
| 168.632 | 2.932 | 150 | 2.50 | | |
| 168.680 | 2.884 | 47 | 0.32 | | |
| 168.711 | 2.853 | 105 | 1.84 | $A1$ | |
| 168.785 | 2.779 | 721 | 0.88 | | |
| 168.850 | 2.714 | 747 | 1.10 | $A2$ | 139 |
| 168.990 | 2.574 | 756 | 1.45 | $A3$ | 140 |
| 169.166 | 2.398 | 318 | 0.20 | | |
| 169.341 | 2.223 | 176 | 0.20 | | |

duce near-perfect fits of the two spectra in this region but would not provide much understanding of the nature of the transitions. An alternative approach was employed instead. The set of adjustable parameters was reduced by making the small set of assumptions described below, which were carefully selected to represent the essential physics of the problem. A least-squares analysis based on these restrictions gave good unique fits of the two spectra when the moleuclar-field splitting of the sulfur $2p_{3/2}$ core levels was included. Much poorer fits were obtained if the $2p_{3/2}$ levels were assumed to be degenerate. Beyond this important result, the analysis correlated each individual absorption feature with one of the three possible $2p$ core holes, thus deconvoluting the Rydberg-orbital structure from the core-level structure. Due to the complexity of the spectrum, the large number of adjustable parameters, and the limited accuracy of the fit, not all the results of this deconvolution are reliable, as discussed in detail below. However, a general understanding of the spectrum is obtained, which might not be apparent otherwise.

For the least-squares analysis of the Rydberg spectra, the following assumptions were applied. (1) The energy spacing of transitions from the three $2p$ core levels to a single Rydberg orbital, i.e., the observed splitting of the three core levels, is independent of which Rydberg orbital is accessed (but see below for a major exception). (2) The

spacing of these triplets is equal for $H_2S$ and $D_2S$. (3) For every pair of transitions $(A,B)$ from the two $2p_{3/2}$ core levels to one Rydberg orbital, the two peaks $A,B$ have equal intensities. Thus, for the triplet of transitions $(A,B,C)$ to a single Rydberg orbital, $A$ and $B$ have equal intensity, but $C$, the transition from the $2p_{1/2}$ level, may have a different intensity. (4) The ratio $X$ of the intensities of peaks $A$ and $C$ [i.e., $X\equiv$(intensity of $A$)/(intensity of $C$)] may vary for different Rydberg orbitals, but must be the same for corresponding triplets in the $H_2S$ and $D_2S$ spectra. (Note that if the intensity ratio between transitions from the $2p_{1/2}$ level and the $2p_{3/2}$ levels follows the spin-orbit "statistical" prediction of 1:2, the ratio $X$ will equal unity.) (5) Each triplet of peaks $(A,B,C)$ must have the same linewidth, which does *not* have to be the same for corresponding triplets in the $H_2S$ and $D_2S$ spectra.

These assumptions warrant some discussion. Assumption (1) is only valid if the Coulombic interaction between the excited electron and the core hole is small. This should apply for the higher Rydberg states, but may be less accurate for the lower Rydberg states. Indeed, this assumption must be relaxed to allow a reasonable fit of the lowest-energy features of Fig. 2, the mixed states, as discussed below. Assumption (2) is valid if the electronic and geometric structure of the final state is essentially the

same in $H_2S$ and $D_2S$. Because the splitting of the $2p_{3/2}$ level is small, the $2p_{3/2}$-$4e_{1/2}$ and $2p_{3/2}$-$5e_{1/2}$ core orbitals must have very similar spatial distributions, supporting assumption (3). Assumption (4) applies because corresponding Rydberg orbitals in $H_2S$ and $D_2S$ should have essentially the same spatial distributions. Note that a deviation of the intensity ratio $X$ from unity indicates a departure from the statistical ratio, which can arise even from a relatively small Coulombic interaction between the core hole and excited electron. $X$ is allowed to vary for different Rydberg orbitals, since differences in the spatial distributions of the various Rydberg orbitals can result in different interactions with the core hole. As discussed below, assumption (4) is not applied to the mixed states, because the correspondence of these features between $H_2S$ and $D_2S$ is difficult to determine. Assumption (5) is only valid if the three core holes decay at the same rate for a given Rydberg excitation. This assumption should apply for the two $2p_{3/2}$ core holes, but might not be accurate for $2p_{1/2}$ vs $2p_{3/2}$ core holes, particularly for the lower Rydberg states. However, this restriction was necessary to keep the number of adjustable parameters in the analysis manageable.

For the analysis, the $H_2S$ and $D_2S$ data sets were fit simultaneously to best exploit assumptions (2) and (4). The fits of the upper Rydberg region, discussed above in Sec. IV B 2, were included in the analysis. Note that this uppermost part of the spectrum, 170.3–171.4 eV, is essentially reproduced twice at lower energies in the fit, to represent the sequence of states approaching the $L_3$-$4e_{1/2}$ and $L_3$-$5e_{1/2}$ edges. This is seen in the three subspectra of Fig. 2 which correspond to the three different core holes. Ideally the three subspectra should be identical except for an energy shift due to the splitting of the $2p$ levels. To obtain a reasonable fit, however, the ratios $X$ for each feature in the subspectra were independently varied within the range 0.20–2.50. The ratios obtained are shown in Tables I and II. For most of the intense features, the derived ratio was close to one. But for some features, including a few intense peaks, significant deviations of $X$ from unity were necessary to obtain a good fit. This is reflected in the subspectra of Fig. 2, where the $(2p_{1/2})^{-1}$ component (dashed line) is, in some areas, different from the lower-energy $(2p_{3/2})^{-1}$ components (solid and dotted lines). Of course the latter two lines are identical, as required by assumption (3). Some of these deviations of $X$ from unity may represent real ratios of transition intensities in the spectrum. Others might be a result of the limited validity of the assumptions (1)–(5), which could force unrealistic values onto some adjustable parameters. Because of this, and also because of the imperfect fit to the data, some of the quantitative results of this least-squares analysis may be unreliable. The results discussed below were selected with these restrictions in mind, and are believed to be valid.

*b. Results of analysis.* Results of the least-squares analysis based on this approach are given in Tables I and II and are plotted as the fits and subspectra in Fig. 2. Due to the large number of adjustable parameters, a simultaneous least-squares fit was not possible. Instead, alternating subsets of parameters were adjusted reitera-

tively until a good fit was obtained. As a result, error bars could not be calculated for the final fit parameters. Some error bars have been estimated, however. The energies, intensities, and intensity ratios (i.e., $X$, as defined above) from the fits are shown in Tables I and II. The only parameters not tabulated are the linewidths of the individual peaks, which have typical values from 75 to 100 meV (Voigt function FWHM). Linewidths are discussed in more detail in Sec. IV D.

Tables I and II give energies of the (S $2p_{1/2})^{-1}$ core-excited states. The term values are obtained by subtraction from the derived sulfur $L_2$ threshold energy of 171.564 eV. The energy of a particular (S $2p_{3/2}$-$4e_{1/2})^{-1}$ or (S $2p_{3/2}$-$5e_{1/2})^{-1}$ core-excited state can be obtained from Table I by subtracting the term value of the corresponding (S $2p_{1/2})^{-1}$ state from the derived values of the $L_3$-$4e_{1/2}$ and $L_3$-$5e_{1/2}$ threshold energies; 170.418 and 170.303 eV, respectively. For the mixed states listed in Table II the term values are derived by assuming the same $L_2$ threshold energy as in Table I. Because different core-level splittings apply for these states (see below), the effective $L_3$-$4e_{1/2}$ and $L_3$-$5e_{1/2}$ threshold energies are 170.471 and 170.432 eV, respectively.

The band of features in the range 167.0–168.2 eV are of special interest because of their dissimilarity in the $H_2S$ and $D_2S$ spectra. Since no sharp, prominent features are observed at lower energies, i.e., in the range 165.8–167.0 eV (see Fig. 3), the transitions within this band must access (S $2p_{3/2})^{-1}$ core-excited states. The corresponding band of (S $2p_{1/2})^{-1}$ states should lie approximately in the range 168.2–169.4 eV, possibly overlapping some (S $2p_{3/2})^{-1}$ core-excited Rydberg states. This rough assignment is supported by the observation of large isotopic differences around 168.7–169.2 eV. The large isotopic differences of the two bands indicate that extensive vibrational excitations accompany these electronic transitions. Thus the features belonging to these two bands are assigned to transitions to mixed orbitals, as discussed in Sec. IV B 1. It should be stressed that the range 168.2–169.4eV includes some (S $2p_{3/2})^{-1}$ core-excited Rydberg states as well as the (S $2p_{1/2})^{-1}$ core-excited mixed states. Deconvoluting these different contributions to the spectra in this and in other regions is one of the main accomplishments of the least-squares analysis.

Without a detailed assignment of the mixed-state transitions for both isotopic species, a reliable one-to-one correlation of the mixed states between $H_2S$ and $D_2S$ is not available because of their large isotopic differences. As a result, assumption (4) was not applied to the mixed states; the intensity ratios used for these peaks are not the same for $H_2S$ and $D_2S$ (see Table II). In order to obtain a good fit to the data, it was also necessary to relax assumption (1) for the mixed states. The mean spin-orbit splitting and the molecular-field splitting used for all of the mixed states were allowed to differ from the splittings used for the Rydberg states, and the overall fit improved dramatically for both $H_2S$ and $D_2S$. This result, along with observation of extensive vibrational excitations, is the main motivation for identifying the states in Table II as intermediate states. The sharp distinction between the mixed

and Rydberg states assumed for this analysis is only an approximation. A more realistic model would allow the splittings of each state to be unique, and the resulting variation of the derived energy splittings would probably be smoother.

For the Rydberg states, the least-squares analysis gave a molecular-field splitting of 115(9) meV and a mean spin-orbit splitting of 1.204(6) eV. (For each quantity, the estimated uncertainty of the last digit is given in parentheses.) These splittings were mainly determined in the fit by the intense features assigned to excitation of $3d$- and $4d$-derived Rydberg states. They are probably also fairly accurate for the higher Rydberg states. For the mixed states, the analysis resulted in a molecular-field splitting of 39(9) meV and a mean spin-orbit splitting of 1.112(6) eV. Thus the molecular-field splitting is 76 meV smaller and the mean spin-orbit splitting is 92 meV smaller in the mixed states, as compared to the Rydberg states. These modified splittings can occur if the direct and/or exchange Coulombic interactions with the sulfur core hole are stronger for an electron in an intermediate-type orbital than they are for an electron in a Rydberg orbital. A *decrease* in the molecular-field splitting of the $2p_{3/2}$ level is not expected, however, when an electron is moved from a Rydberg orbital to an orbital with *more* valence character. Although it is difficult to interpret, the reduced molecular-field splitting in the mixed states is a firm result of the analysis. Indeed, if the derived Rydberg-state splitting applied also to the mixed states, the transitions to the (S $2p_{3/2}$)$^{-1}$ mixed states ($\approx 167-168.2$ eV) in $H_2S$ and especially $D_2S$ would have a pronounced doublet structure which is not, in fact, observed. The derived decrease in mean spin-orbit splitting for the mixed states is discussed in the next section.

The derived Rydberg-state splittings may include some direct- and exchange-interaction contributions, but they nonetheless can be compared to recent measurements made by Svensson et al., using high-resolution XPS and AES [16]. In that paper, a small difference was reported between the spin-orbit splitting of the $H_2S$ sulfur $2p$ level as measured by XPS and by AES. These results were explained, in part, by estimating the molecular-field splitting of the sulfur $2p_{3/2}$ level to be $\approx 106$ meV in the core-excited ion. The mean spin-orbit splitting measured by XPS was 1.201 eV. These values are in very good agreement with the corresponding quantities measured in the present experiment for the core-excited Rydberg states, suggesting that the interpretation of Svensson et al. is valid and also that Coulombic interactions do not affect the measured splittings very much for the Rydberg states. Svensson et al. do not provide absolute binding energies, but the sulfur $2p$ binding energies (170.22 eV, 171.42 eV) measured by XPS with lower resolution in Ref. [18] are within 0.2 eV of the derived sulfur $2p$ ionization thresholds listed in Table I. The sulfur $2p$ spin-orbit splitting obtained in Ref. [18] (1.20 eV) agrees with the mean spin-orbit splitting derived here (1.204 eV).

As a test, an alternate least-squares analysis of the data was performed with the molecular-field splitting of the $2p_{3/2}$ level fixed at zero. Otherwise this "no-splitting" test analysis was subject to exactly the same freedoms

and restrictions as the "split" fit. Thus the split fit had only *two* more adjustable parameters than the no-splitting fit; the $2p_{3/2}$ splitting of the Rydberg states and of the mixed states. The results of the no-splitting fit (not shown) are not nearly as convincing as the results of the split fit presented above. Most notably, the regions around 169.0–169.4 and 169.8–170.2 eV are poorly approximated by the no-splitting fit. Besides giving a poorer fit, the derived parameters are more difficult to interpret. The intensity ratios of the more intense features show significantly larger deviations from unity in the no-splitting fit than in the split fit presented here in Tables I and II. For example, in the no-splitting fit for $H_2S$ ($D_2S$), five of the ten most intense features have a ratio outside the range 0.7–2.4 (0.5–2.4). By comparison, in the split fit for $H_2S$ ($D_2S$), only one (two) of the ten most intense features have a ratio outside the *narrower* ranges 0.7–1.2 (0.7–1.5). As mentioned above, some deviation of the intensity ratio $X$ from unity is plausible, but when ratios for many intense peaks assume values much smaller or larger than one, with no apparent pattern, the validity of the analysis is questionable. The results of the no-splitting fit are much poorer than would be expected merely from reducing the total number of adjustable parameters by two, as compared to the split fit. This test therefore provides substantial evidence for the molecular-field splitting of the $2p_{3/2}$ core level. The unambiguous identification of the $2p_{3/2}$ molecular-field splitting in this spectrum is, in fact, the most significant result of this paper.

Just below threshold, the Rydberg formula successfully predicts the energies of the transitions, as discussed in Sec. IV B 2. The quantum defects obtained from this analysis can be used to roughly characterize the lower-energy core-excited states. Using the quantum defect determined from the energies of the $(2p_{1/2})^{-1}$ $nd$ ($n = 5-8$) Rydberg states, the term value of the $2p^{-1}$ $3d$ state is predicted to be 1.89 eV. As shown in Table I, there are several intense transitions with term values close to this prediction. They have therefore been assigned as "$3d$ derived"; i.e., they arise from several molecular core-excited states which can be associated with the atomic $2p^{-1}$ $3d$ state. Similarly, there are several $4d$-derived states (see Sec. IV B 2), but they are spread over a narrower energy range as compared to the $3d$-derived states, because they have a larger spatial extent and are influenced less by the molecular field.

Based upon the energy of the $(2p_{1/2})^{-1}$ $6s$ state, the $5s$ state should have a term value of $\approx 1.6$ eV. A medium-intensity feature with this term value has been tentatively assigned to a $5s$-derived state. The $4s$ state is predicted at a term value of $\approx 3.8$ eV, and may be contributing to the mixed states at somewhat lower term values and/or to the valence-shell states at somewhat higher term values. The defect determined from the energies of the $2p^{-1}$ $np$ ($n = 6-8$) Rydberg states predicts a term value of 2.43 eV for the $2p^{-1}$ $4p$ states. Table II shows that the spectra of both $H_2S$ and $D_2S$ have bands centered at slightly higher term values (lower transition energies). These bands include significant vibrational excitations, so the average term values of the electronic states must be even higher than the band center. This is consistent with the assign-

ment of this band to mixed states, because the valence contribution to these states could shift them to higher term values than expected for pure $4p$-derived Rydberg states. It should be stressed that, for the states in these spectra with term values greater than $\approx 1$ eV, the association with a specific atomic Rydberg state is approximate at best. In fact, states which share the same total symmetry and similar energies can mix, and thus a *single* core-excited state may be derived from a *combination* of atomic $s$, $p$, and $d$ states. Indeed, it is the mixing of $d$ character into the $p$ states which gives the $p$ series appreciable intensity in the near-threshold region [34].

### 4. Comparison to other XANES spectra

*a. Mixed states.* Comparison to a related XANES spectrum is especially useful for the interpretation of the splittings of the mixed states in $H_2S$. The sulfur $L_{2,3}$ XANES spectrum of $SF_6$ was recently measured with high energy resolution using the same experimental apparatus as the present measurements [10]. The spectrum showed intense transitions to the $(S\ 2p)^{-1}\ a_{1g}$ valence-shell states as well as much weaker transitions to $(S\ 2p)^{-1}$ $nl$ Rydberg states. The Rydberg states with the largest term value, $(S\ 2p_{1/2,3/2})^{-1}\ 4s$, showed the same spin-orbit splitting as the higher Rydberg states, weak vibrational excitations, and only a very small deviation from the energy predicted by the quantum defect of the higher $ns$ states. It therefore appears that there are no $2p$-excited mixed states in this molecule, presumably because the large potential barrier created by the fluorine "cage" prevents the interaction of valence and Rydberg orbitals. This is in distinct contrast to $H_2S$, where the hydrogen atoms are not expected to create an appreciable potential barrier, and relatively intense transitions to mixed states are observed.

The comparison of the $(S\ 2p)^{-1}$ Rydberg states and the $(S\ 2p)^{-1}\ a_{1g}$ valence-shell states in $SF_6$ is particularly relevant here. A slightly smaller spin-orbit splitting was measured for the valence-shell states, as compared to the splitting of the Rydberg states. (Note that molecular-field splitting of the sulfur $2p_{3/2}$ levels is not possible in $SF_6$ because of the octahedral symmetry.) Because of good spatial overlap, the exchange interaction of the excited electron with the core hole is larger in the valence-shell states than in the Rydberg states, and the dependence of that interaction on the $j$ value of the core hole reduces the observed spin-orbit splitting. The observed shift of $\approx -30$ meV in $SF_6$ [10] is smaller than the effect observed in $H_2S$ for the mean spin-orbit splitting of the mixed states (shift equals $-92$ meV, relative to the Rydberg-state value). The exchange interaction in $SF_6$ for the valence-shell states has a much greater effect upon the intensity ratio of the two $(S\ 2p_{1/2,3/2})^{-1}\ a_{1g}$ transitions than it does upon the spin-orbit splitting. Similar behavior is also seen in spectra of the xenon fluorides, and was predicted by calculations [35]. The measured ratio in $SF_6$ was 0.62 $(2p_{3/2}^{-1}:2p_{1/2}^{-1})$ for the valence-shell states as compared to 2.1 for the Rydberg states [36]. (Note that the statistical ratio, expected in the limit of no exchange interaction, is 2.00, corresponding to an intensi-

ty ratio of $X=1.00$ in the notation used here for $H_2S$.) Summing the intensities of all the mixed states, the overall intensity ratio $X=1.03$ (1.04) is obtained for $H_2S$ ($D_2S$). For the summed Rydberg states, the overall intensity ratio is $X=1.03$ (1.01) for $H_2S$ ($D_2S$). These ratios are estimated to be accurate to within $\approx 5\%$, despite the limitations of the analysis.

The behavior of the mixed states in $H_2S$ is thus quite different from that of the valence-shell states in $SF_6$: the mean spin-orbit splitting differs significantly from the Rydberg value but the intensity ratio deviates very little from the statistical value. This suggests that a larger exchange interaction in the mixed states is not the primary cause of the change in mean spin-orbit splitting, relative to the Rydberg states. This change may also result from the lower symmetry of $H_2S$, which allows the observed mean spin-orbit splitting to have contributions from the direct Coulombic interaction of the excited electron with the core hole; this is not possible in the high-symmetry $SF_6$ molecule. These direct interactions scale with the spatial overlap of the excited electron and the core hole, and thus should be small for the Rydberg states, but larger for the mixed states. The change in the mean spin-orbit splitting observed for the mixed states of $H_2S$, compared to the Rydberg states, is tentatively attributed to a difference in the direct interaction of the excited electron with the $(2p_{3/2})^{-1}$ and $(2p_{1/2})^{-1}$ core holes. An accurate theoretical treatment which includes all possible effects is necessary for a more definite understanding of these splittings.

*b. Rydberg states.* One result of the assignments of the upper Rydberg states given in Sec. IV B 2 and Table I is perhaps surprising: the intensities of transitions to the $5p$ and $6p$ orbitals are comparable to those for the $5s$ and $6s$ orbitals. In atomic dipole-selection rules, the $2p$ to $np$ transition is forbidden. Since higher Rydberg orbitals are increasingly atomiclike, it might be expected that these transitions would be very weak in $H_2S$. What instead occurs is that, because of the nonspherical molecular symmetry, the $p$ orbitals mix with the $d$ orbitals and "borrow" intensity from the very favorable $2p$ to $nd$ transitions [34]. A similar situation is found in the $L_{2,3}$ spectrum of the isoelectronic molecule HCl [22,37], where the $2p^{-1}$ $4p$-derived excitation is quite intense. The quantum defects derived in Ref. [37] for HCl ($\delta_s=2.12$, $\delta_p=1.7$, $\delta_d=0.3$) are in excellent agreement with those given here for $H_2S$ ($\delta_s=2.10$, $\delta_p=1.63$, $\delta_d=0.32$). The success of a similar model in both molecules supports the validity of the assignments. Further support comes from the high-resolution $L_{2,3}$ spectrum of the isoelectronic atom argon [2,29]. The quantum defects determined for Ar in Ref. [29] ($\delta_s=2.2$, $\delta_p=1.74$, $\delta_d=0.2$) are in good agreement with those of $H_2S$ and HCl. Note that, as a result of the multipolar nature of electron-energy-loss (EELS) excitations, the dipole-forbidden transition to the $(2p_{3/2})^{-1}$ $4p$ state was observed in Ref. [29].

### 5. Comparison to previous $H_2S$ results

An $L_{2,3}$ near-edge spectrum of $D_2S$ has not been previously published. The $H_2S$ spectrum shown here shows

significant improvements over earlier published spectra. Recently a spectrum was published [5] with slightly worse resolution and a poorer signal-to-noise ratio, and no attempt was made to assign the peaks or analyze the spectrum. The first experimental results were presented by Hayes and Brown [12]. Due to limited resolution, only the general outline of the spectrum was seen, without the extensive fine structure now observed. The initial assignments of Hayes and Brown were later reassessed by Robin [14] and Schwarz [13]. Both of these later assignments attributed the broad features at lowest energies to valence-shell excitations. The higher-energy features were assigned to $s$, $p$ and $d$ Rydberg states. Schwarz, in particular, assigned all observed features in a manner consistent with his assignments for the corresponding spectra of other third-row hydrides. The present assignments, made in the light of considerably more resolved peaks and a detailed analysis, agree with Schwarz in the assignment of the $6a_1$, $3b_2$, and $d$ Rydberg states. Schwarz's $5s$ and $6s$ states are attributed here to $p$-type states, resulting in consistent quantum defects as discussed in the preceding section. The $4s$ and $4p$ states are not explicitly assigned here, because the strong influence of the molecular field makes these atomic designations inapplicable. However, the mixed states identified here can be loosely attributed to $4p$ and $4s$ atomic parentage (see Sec. IV B 3 b), which is then in agreement with Schwarz's assignment.

### 6. Vibrational structure

A direct comparison of the two spectra in Fig. 2 identifies the features which arise from vibrational excitations, because of the isotopic dependence of vibrational spacings. The least-squares fit analysis of the spectra essentially deconvolutes the effects of the core-level splittings. The term values obtained are listed in Tables I and II; differences between those of $H_2S$ and $D_2S$ may be attributed to vibrational sidebands. Weak vibrational excitations, probably of the $v_1$ symmetric stretch mode (ground-state spacing equals 324 meV [33]), were observed in photoelectron spectra from the $2p$ levels of $H_2S$, with a branching ratio of $\approx 5\%$ for the first vibrational peak [18]. Because of that result, similar excitations are expected for the higher Rydberg states in the present measurements. No such excitation was observed, however, possibly because of the small branching ratio. As mentioned in Sec. IV B 2, the $(S\ 2p_{1/2})^{-1}\ 5p,4d$ region shows a small vibrational sideband probably associated with the $v_2$ bend mode.

The peak at $\approx 169.55$ eV has noticeably larger intensity in the $D_2S$ spectrum, but the results of the analysis do not suggest any simple vibrational explanation. Those results may be somewhat inaccurate considering the unusually small intensity ratio ($X=0.2$) obtained for one of the two states contributing to this $3d$-derived feature, as well as the small intensity ratios for the states at 168.37 eV which overlap the $(2p_{3/2})^{-1}$ states of this $3d$-derived feature.

The mixed states show the most obvious isotopic effects in the spectra. The derived term values in Table II

show some regular spacing, indicated by the labels $A\,1$, $A\,2$, etc. For $H_2S$, a spacing of $\approx 155$ meV is apparent from the results of the fit, presumably due to a vibrational progression in the $v_2$ bend mode, which has a ground-state spacing of 147 meV [33]. Regular spacings are much less evident in the $D_2S$ results, but a spacing of 140 meV is observed, possibly corresponding to the $v_2$ bend mode, which has a ground-state spacing of 106 meV [33]. For neither molecule is there a simple way to assign all the states to vibrational progressions of a single electronic transition. Instead, there seem to be at least two electronic transitions in this energy range. The difficulty in interpreting the spectra even as *several* overlapping vibrational progressions could arise from strong vibronic coupling between two or more electronic states. These interactions can produce irregular fine structure in absorption spectra [38].

### C. Sulfur $L_{2,3}$ edges: Valence-shell excitations

#### 1. Assignment and electron-hole interaction

The broad, overlapping peaks shown in Fig. 3 are assigned to one-electron excitations from the sulfur $2p$ core levels to the $6a_1$ and $3b_2$ molecular orbitals, in agreement with previous reports [13,14]. A recent calculation predicted the $3b_2$ orbital to have lower energy than $6a_1$ in the presence of a $2p$ core hole [39]. The opposite order $6a_1 < 3b_2$ calculated in Refs. [13,24,27] will be assumed here. A simple extension of the discussion in Sec. IV B 1 shows that 18 dipole-allowed final states result from the combination of the two unoccupied molecular orbitals with the three possible core levels which may excite them. In fact, as seen above for the Rydberg states, many of these electronic states are nearly degenerate.

As discussed above in Sec. IV B 4 a, the spin-orbit splittings and intensity ratios of core-excited valence-shell states are expected to show the effect of the exchange interaction (and possibly the direct interaction) between the core hole and excited electron. To characterize these effects in the spectra of Fig. 3, approximate fits were made to the data. The absorption features between 163 and 167 eV were modeled by two doublets, with splittings arbitrarily set equal, described by four very broad Gaussian peaks. The Gaussian line shape roughly approximates the broadening due to unresolved or barely resolved vibrational progressions. The four peaks represent the states, in order of increasing energy, which roughly account for the actual spectrum: $(2p_{3/2})^{-1}\ 6a_1$, $(2p_{3/2})^{-1}\ 3b_2$, $(2p_{1/2})^{-1}\ 6a_1$, and $(2p_{1/2})^{-1}\ 3b_2$.

A least-squares fit analysis based on this simple model gave spin-orbit splittings of 1.07 eV (1.09 eV) for $H_2S$ ($D_2S$). These values are slightly smaller than the mean spin-orbit splitting determined for the mixed states and significantly smaller than the mean spin-orbit splitting determined for the Rydberg states. This supports the expectation, based upon arguments of spatial overlap, that Coulombic interactions between the core hole and excited electron are most significant for the core-excited valence-shell states, less so for the core-excited mixed states, and least important for the core-excited Rydberg states.

The statistical intensity ratio, $(2p_{3/2}^{-1}:2p_{1/2}^{-1})=2.00$, is expected if the spin-orbit interaction dominates. The intensity ratios derived from the analysis were $[(2p_{3/2})^{-1} 6a_1:(2p_{1/2})^{-1} 6a_1]=1.8(2.1)$ and $[(2p_{3/2})^{-1} 3b_2:(2p_{1/2})^{-1} 3b_2]=1.2$ (1.1) for $H_2S$ ($D_2S$). The derived values for the $3b_2$ excitations are much less than the statistical value, indicating that Coulombic interactions are largest for those states. Similar deviations of the intensity ratio from the statistical value have been observed in the corresponding core-excited valence-shell states of other third-row hydrides [13,40]. While the quantitative results of this rough analysis may be unreliable, the qualitative trends in splittings and intensity observed here very likely reflect real effects.

### 2. Vibrational structure and other isotopic shifts

The spectra of Fig. 3 show some regularly spaced fine structure, more easily observed in the expanded insets, with a notable isotopic dependence. A comparison of the two spectra also reveals small differences in the overall line shape and peak position. The dissociative nature of the excited electronic states must be considered in the interpretation of these results. Recent photoion [25] and Auger-electron [26,27] studies have clearly shown that rapid predissociation is the dominant decay process for these core-excited valence-shell states. The core-excited molecule fragments into H and HS* with a rate faster than the Auger decay of the $2p$ core hole. There has been considerable interest in lower-energy dissociative electronic states of $H_2S$ [41–43]. Specifically, the broad peak in the uv absorption spectrum centered at $\approx 195$ nm is known to correspond to a dissociating state [42]. This peak shows isotopic-dependent weak fine structure which is strikingly similar to the structure of Fig. 3. This similarity may result from analogous electronic configurations; the 195-nm band corresponds to the excitation of the outermost ground-state electron, in the nonbonding $2b_1$ orbital, to the $6a_1$ orbital. The transition to the $3b_2$ orbital is dipole forbidden, but that excited state strongly influences the observed spectrum through vibronic coupling [43].

A comparison of the two spectra in Fig. 3 shows a shift of the leading edge of the peak to higher energy in $D_2S$. Both the peak maximum and the trailing edge show a shift to lower energy in $D_2S$, discussed below. To illustrate these shifts, Fig. 3 indicates the energies of the peak maxima and the leading- and trailing-edge inflection points with vertical lines. The shift of the leading edge is expected for a direct transition to a dissociative electronic state. The potential surface of such an excited state does not support vibrational states for the asymmetric-stretch mode, and there is no contribution to the total energy of the excited state from the zero-point energy of this mode. The zero-point energy of this mode does contribute to the energy of the *ground* state, and that contribution is half the harmonic vibrational energy. The harmonic energies are 337 meV for $H_2S$ and $\approx 249$ meV for $D_2S$ [33]. The observed transition energy to a dissociative electronic state should therefore be $(\frac{1}{2})\times(337-249)$ $=44$ meV larger for $D_2S$. This agrees with the observed

shift of $+0.05(2)$ eV for the leading-edge inflection point in $D_2S$ as compared to $H_2S$. The leading-edge region of the peak is dominated by transitions to the $(2p_{3/2})^{-1} 6a_1$ state, which was calculated to be dissociative by Naves de Brito and Agren [27]. It should be noted that changes in the spacings of the other two vibrational modes upon excitation also have an effect on transition energies. The zero-point differences of these modes may also contribute to the observed shift, but to a lesser extent than the asymmetric-stretch mode.

A series of Voigt functions were used in a least-squares analysis to fit the weak fine structure observed in the range $\approx 165.0–165.7$ eV for both $H_2S$ and $D_2S$. Only a linear background was employed; i.e., possible contributions from broader overlapping peaks were not included. The results of this analysis are plotted with the data in the expanded portion of Fig. 3 and listed in Table III. In principle, the individual peaks barely resolved in the spectra could be vibrational sidebands of more than one electronic transition. In the region of the vibrational structure the strongest contributions are probably from the $(S\ 2p_{3/2})^{-1} 3b_2$ state. Weaker contributions from the $(S\ 2p_{1/2})^{-1} 6a_1$ and $(S\ 2p_{3/2})^{-1} 6a_1$ states are also possible. These designations are only approximate; as many as 15 distinct electronic states could in fact contribute in this range. Assuming that the sidebands are a single progression from only *one* electronic transition gives reasonable results, however. This suggests that much of the possible electronic splitting is not actually large enough to affect the spectrum. In particular, the molecular-field splitting of the $2p_{3/2}$ level must be less than $\approx 50$ meV, notably smaller than the value derived for the upper Rydberg states. The average spacing determined for the peaks in this range is 167(3) meV for $H_2S$ and 145(3) meV for $D_2S$.

The interpretation of an apparent vibrational progression in the excitation of a dissociative state is especially difficult in the present case where vibronic coupling may have a significant influence. Using the following arguments, which are based upon previously published results, the observed progression is tentatively assigned to excitation of the $v_1$ symmetric-stretch mode of the $(2p_{3/2})^{-1} 3b_2$ state. The calculations of the $(2p)^{-1} 6a_1$ and $(2p)^{-1} 3b_2$ hypersurfaces by Naves de Brito and Agren [27] are particularly useful here. They found that the $(2p)^{-1} 3b_2$ excited state, at higher energy, is bound, but strongly vibronically coupled to the dissociative $(2p)^{-1} 6a_1$ state. Assuming this model, there are two possible origins for the observed vibrational structure. (1) Excitation of the dissociative $(2p)^{-1} 6a_1$ state may exhibit a diffuse vibrational progression in a nondissociative mode [44]. (2) The vibrational states may reside on the bound $(2p)^{-1} 3b_2$ potential, before the system crosses to the dissociative potential. The latter explanation, for lower-energy states, was recently obtained by Schinke and co-workers from calculations of the fine structure in the 195-nm band of $H_2S$ [43]. They attribute the observed progression to the excitation of the $v_1$ symmetric-stretch mode in a bound state, which is strongly vibronically coupled to a dissociative state at lower energy. This

result is somewhat unexpected, because the observed spacings in the 195-nm band of $H_2S$ and $D_2S$ are almost exactly equal to the corresponding $v_2$ symmetric-*bend* mode spacings of the ground state.

Based only on their derived spacings in Table III, the peaks of Fig. 3 might be attributed to a progression in the $v_2$ bending mode, which has a spacing of 147 and 106 meV in the ground state of $H_2S$ and $D_2S$, respectively [33]. The results of Schinke and co-workers [43] suggest the alternate possibility that the progression is associated with a much-softened $v_1$ symmetric-stretch mode, which as a spacing of 324 and 235 meV in the ground state of $H_2S$ and $D_2S$, respectively [33]. Indeed, the bound $(2p)^{-1}$ $3b_2$ potential calculated by Naves de Brito and Agren [27] appears to have a much smaller slope (i.e., smaller force constant) in the direction of the symmetric stretch as compared to the calculated ground-state potential. Thus the vibrational progression observed here is tentatively assigned to the $v_1$ symmetric-stretch mode of the $(2p_{3/2})^{-1} 3b_2$ state.

A corresponding progression of the $(2p_{1/2})^{-1} 3b_2$ state was not clearly resolved, but a second-derivative analysis of the spectra identified some regularly spaced fine structure in the range $\approx 166.3–166.9$ eV, with a spacing of $\approx 154$ meV ($\approx 127$ meV) for $H_2S$ ($D_2S$). The lack of distinct fine structure for the $(2p_{1/2})^{-1} 3b_2$ state may reflect a larger natural linewidth than for the $(2p_{3/2})^{-1} 3b_2$ state, perhaps because this higher-energy state has access to additional decay channels. The ratio of vibrational spacings in the $(2p_{3/2})^{-1} 3b_2$ excited state is 0.87(3) ($D_2S:H_2S$), as compared to 0.72 in the ground state for the $v_1$ mode (and the $v_2$ mode). This difference indicates an isotopic dependence of the potential surfaces. This could result from the strong vibronic coupling between the electronic states predicted by Naves de Brito and Agren for the region of the vertical transition.

Portions of the spectra in Fig. 3 are attributed to the excitations of bound states, which are accompanied by progressions of vibrational excitations. The resulting contributions to the observed spectrum are broad bands, each composed of a series of individual vibronic peaks. Therefore the center of such a band should shift to lower energies for $D_2S$, because of the smaller vibrational spacings as compared to $H_2S$. This explains the shifts of the peak maximum and the trailing-edge inflection point in-

dicated in Fig. 3, which are $-0.08(1)$ and $-0.05(3)$ eV (for $D_2S$ as compared to $H_2S$) and are mainly associated with the $(2p_{3/2})^{-1} 3b_2$ and $(2p_{1/2})^{-1} 3b_2$ states, respectively. These shifts may also include contributions from vibrational zero-point energy changes, as described above, which are expected to be positive and less than $\approx 0.05$ eV for these bound states.

### D. Linewidths

The least-squares fit presented in Table III and in Fig. 3 gave an excellent fit to the fine structure of the valence-shell states, suggesting that the derived parameters have physical significance. Assuming an instrumental linewidth of 30 meV (Gaussian FWHM), the derived natural linewidths (Lorentzian FWHM) for the individual vibrational peaks in the fit are 344(15) meV for $H_2S$ and 306(15) meV for $D_2S$. Although the difference is not much larger than the error bars, the implication is that these core-excited valence-shell states decay faster for $H_2S$ than for $D_2S$, an isotopic dependence which is unexpected for the Auger decay process. This result is consistent with the assignment of this fine structure to vibrations of a bound state, which is rapidly depopulated by vibronic coupling to a dissociative state. The observed isotopic lifetime dependence indicates that the vibronic coupling is somewhat weaker for $D_2S$.

These valence-shell excitation natural linewidths are much larger than those derived for the Rydberg excitations. For example, assuming an instrumental linewidth of 30 meV at $h\nu = 171$ eV, the derived natural linewidths for $H_2S$ are 65(7) and 51(7) meV for the $(2p_{1/2})^{-1} 7d$ and $(2p_{1/2})^{-1} 8d$ states, respectively, compared with 344 meV for the valence-shell states. This trend is consistent with the decreasing evidence of predissociation observed by photoion spectroscopy as the excitation energy was increased into the Rydberg region of the photoabsorption spectrum [25]. The predissociation of the valence-shell excitations in $H_2S$ precludes a direct comparison to the corresponding states of $SF_6$. The derived natural linewidths of the Rydberg excitations may be compared, however, after accounting for a revised estimate of instrumental resolution (33 meV at $h\nu = 180$ eV) since the publication of the $SF_6$ results. The narrowest natural linewidth for $H_2S$ is 51(7) meV, compared to 35(8) meV in $SF_6$. The difference reflects the effect of chemical substituents on the electron density at the sulfur core: six fluorine atoms will withdraw much more electron density than two hydrogen atoms, resulting in a much-reduced rate of Auger decay. The calculated natural linewidth for atomic sulfur is 54 meV [45], very close to the minimum value measured for $H_2S$.

### E. Comparison to theoretical results

Comparisons to theoretical work have been mentioned, as appropriate, in the preceding sections. Only a few points need further comment here. There have been several theoretical studies of the $L_{2,3}$ XANES spectrum of $H_2S$ [13,24,34,39]. While none of these theoretical results accurately predict the fine structure observed in the

TABLE III. Results of least-squares analysis of $L_{2,3}$ valence-shell region: Exact fit of fine structure. Energies of peaks, with uncertainties, and energy spacings between successive peaks are tabulated for $H_2S$ and $D_2S$.

| H₂S | | D₂S | |
|---|---|---|---|
| Energy (eV) | Spacing (meV) | Energy (eV) | Spacing (meV) |
| 165.037(9) | | 164.998(9) | |
| 165.204(6) | 167 | 165.146(8) | 148 |
| 165.371(7) | 167 | 165.289(7) | 143 |
| 165.536(9) | 165 | 165.428(7) | 139 |
| 165.706(9) | 170 | 165.577(9) | 149 |

preset measurements, some of these results were used as a guide in the assignments given here. Specifically, Schwarz [13] and Cacelli, Carravetta, and Moccia [24] both predict transitions to $4p$-derived orbitals with term values of $\approx 2.4$ eV, as also predicted by the quantum defect derived here for the higher $np$ orbitals. These results suggest a strong $4p$ contribution to the mixed states. Cacelli, Caravetta, and Moccia predict relatively intense transitions to orbitals having mainly $3d$ and $5s$ contributions with term values of $\approx 1.7–2.0$ eV, again in agreement with the predictions of quantum defects derived here for the higher Rydberg orbitals. Recent calculations by Liu, Bancroft, and Tse [34] suggest that transitions to the higher $np$ orbitals have appreciable intensity. This supports the assignment deduced here primarily on the basis of consistent quantum defects.

In one calculation, the molecular-field splitting of the sulfur $2p_{3/2}$ level was predicted to be 44 meV for core-ionized $H_2S^+$ [46]. Another calculation estimated that splitting to be 80 meV [47]. Because the Rydberg electron should have only a small influence at the atomic core, these values can be compared to the 115-meV splitting derived here for the Rydberg states. Agreement with the calculations is fair, considering the $\approx 170$-eV total energy of the excited state.

## V. CONCLUSIONS

In the present work, the high-resolution low-noise XANES spectrum of $H_2S$ below the sulfur $L_{2,3}$ edges was measured, providing significant improvements over previous measurements. Analysis of these spectra clearly indicated that the sulfur $2p_{3/2}$ core level is split into two levels by the anisotropic molecular field. That splitting is measured to be 115 meV for the Rydberg excitations, in good agreement with the splitting proposed for the core-ionized molecule based on high-resolution XPS and AES spectra [16]. The comparison of the $H_2S$ spectrum to the corresponding $D_2S$ spectrum was essential for the identification of vibrational excitations. Quantum defects derived for the higher Rydberg orbitals were similar to the quantum defects from the corresponding spectra of the isoelectronic systems HCl and Ar. Fine structure was observed for the transitions to the dissociative valence-shell states. The regular spacing and isotopic dependence of this structure clearly identifies it as a vibrational progression.

A sophisticated least-squares analysis was applied to the data, allowing the deconvolution of core-level and excited-orbital splittings. This approach will also be useful for the analysis of complex high-resolution XANES spectra of other molecules. Although the resulting fits of the Rydberg and mixed regions of the spectra are unique and accurate within the stated assumptions, and those assumptions are believed to be the best possible, the present interpretation has some limitations. Higher-resolution XANES measurements might help to establish a better understanding of the spectra, but more detailed experiments are probably also required. For example, if Auger-electron spectra are measured using high-resolution photoexcitation, the autoionization processes of individual states in the spectrum may be distinguished, providing more information on the differences between these states.

## ACKNOWLEDGMENTS

[1] K. Siegbahn, C. Nordling, G. Johansson, J. Hedman, P. F. Hedén, K. Hamrin, U. Gelius, and T. Bergmark, *ESCA Applied to Free Molecules* (North-Holland, Amsterdam, 1969), pp. 104–136; D. A. Shirley, Chem. Phys. Lett. **16**, 220 (1972); U. Gelius, Phys. Scr. **9**, 133 (1974); L. Asplund, P. Kelfve, H. Siegbahn, O. Goscinski, H. Fellner-Feldegg, K. Hamrin, B. Blomster, and K. Siegbahn, Chem. Phys. Lett. **40**, 353 (1976); N. D. Lang and A. R. Williams, Phys. Rev. B **16**, 2408 (1977).

[2] M. Domke, T. Mandel, A. Puschmann, C. Xue, D. A. Shirley, G. Kaindl, H. Petersen, and P. Kuske, Rev. Sci. Instrum. **63**, 80 (1992).

[3] M. Domke, A. Puschmann, C. Xue, D. A. Shirley, G. Kaindl, and H. Petersen, Synchrotron Radiat. News **3** (5), 15 (1990).

[4] P. A. Heimann, F. Senf, W. McKinney, M. Howells, R. D. van Zee, L. J. Medhurst, T. Lauritzen, J. Chin, J. Meneghetti, W. Gath, H. Hogrefe, and D. A. Shirley, Phys. Scr. **T31**, 127 (1990); C. T. Chen and F. Sette, Rev. Sci. Instrum. **60**, 1616 (1989); H. Maezaura, A. Toyoshima, Y. Kagoshima, K. Mari, and T. Ishikawa, *ibid.* **60**, 1889 (1989).

[5] D. Thomas, M. Coville, R. Thissen, and P. Morin, Synchrotron Radiat. News **5** (3), 9 (1992).

[6] C. T. Chen, Y. Ma, and F. Sette, Phys. Rev. A **40**, 6737 (1989).

[7] M. Domke, C. Xue, A. Puschmann, T. Mandel, E. Hudson, D. A. Shirley, and G. Kaindl, Chem. Phys. Lett. **173**, 122 (1990); **174**, 668 (1990).

[8] F. X. Gadea, H. Köppel, J. Schirmer, L. S. Cederbaum, K. J. Randall, A. M. Bradshaw, Y. Ma, F. Sette, and C. T. Chen, Phys. Rev. Lett. **66**, 883 (1991).

[9] G. Remmers, M. Domke, A. Puschmann, T. Mandel, C. Xue, G. Kaindl, E. Hudson, and D. A. Shirley, Phys. Rev. A **46**, 3935 (1992).

[10] E. Hudson, D. A. Shirley, M. Domke, A. Puschmann, G. Remmers, T. Mandel, C. Xue, and G. Kaindl, Phys. Rev. A **47**, 361 (1993).

[11] Y. Ma, C. T. Chen, G. Meigs, K. Randall, and F. Sette, Phys. Rev. A **44**, 1848 (1991); J. Schirmer, A. B. Trofimov, K. J. Randall, J. Feldhaus, A. M. Bradshaw, Y. Ma, C. T. Chen, and F. Sette, *ibid.* **47**, 1136 (1993); G. Remmers, M. Domke, and G. Kaindl, *ibid.* **47**, 3085 (1993).

[12] W. Hayes and F. C. Brown, Phys. Rev. A **6**, 21 (1972).

[13] W. H. E. Schwarz, Chem. Phys. **11**, 217 (1975).

[14] M. B. Robin, Chem. Phys. Lett. **31**, 140 (1975).

[15] C. Sandorfy, Top. Curr. Chem. **86**, 91 (1979).

[16] S. Svensson, A. Naves de Brito, M. P. Keane, N. Correia, and L. Karlsson, Phys. Rev. A **43**, 6441 (1991).

[17] K. Siegbahn, C. Nordling, G. Johansson, J. Hedman, P. F. Hedén, K. Hamrin, U. Gelius, and T. Bergmark, *ESCA Applied to Free Molecules* (North-Holland, Amsterdam, 1969), pp. 84–87.

[18] R. G. Cavell and K. H. Tan, Chem. Phys. Lett. **197**, 161 (1992).

[19] F. J. Comes, R. Haensel, U. Nielson, and W. H. E. Schwarz, J. Chem. Phys. **58**, 516 (1973).

[20] R. P. Gupta, J. S. Tse, and G. M. Bancroft, Philos. Trans. R. Soc. Ser. A **293**, 535 (1980); G. M. Bancroft and J. S. Tse, Comments Inorg. Chem. **5**, 89 (1986); J. N. Cutler, G. M. Bancroft, and K. H. Tan, J. Chem. Phys. **97**, 7932 (1992).

[21] K. Ninomiya, E. Ishiguro, S. Iwata, A. Mikuni, and T. Sasaki, J. Phys. B **14**, 1777 (1981).

[22] E. Ishiguro, S. Iwata, A. Mikuni, Y. Suzuki, H. Kanamori, and T. Sasaki, J. Phys. B **20**, 4725 (1987).

[23] N. A. Shklyaeva, L. N. Mazalov, and V. V. Murakhtanov, J. Struct. Chem. **20**, 621 (1979); K. H. Sze, C. E. Brion, X. M. Tong, and J. M. Li, Chem. Phys. **115**, 433 (1987).

[24] I. Cacelli, V. Carravetta, and R. Moccia, Chem. Phys. **120**, 51 (1988).

[25] P. Morin, M. Lavollée, and M. Simon (unpublished).

[26] H. Aksela, S. Aksela, A. Naves de Brito, G. M. Bancroft, and K. H. Tan, Phys. Rev. A **45**, 7948 (1992).

[27] A. N. de Brito and H. Agren, Phys. Rev. A **45**, 7953 (1992).

[28] R. N. S. Sodhi and C. E. Brion, J. Electron Spectrosc. Relat. Phenom. **34**, 363 (1984).

[29] G. C. King, M. Tronc, F. H. Read, and R. C. Bradford, J. Phys. B **10**, 2479 (1977).

[30] R. L. Cook, F. C. DeLucia, and P. Helminger, J. Mol. Struct. **28**, 237 (1975).

[31] G. Herzberg, *Molecular Spectra and Molecular Structure* (Van Nostrand Reinhold, New York, 1966), Vol. III, pp. 17 and 18.

[32] U. Fano and J. W. Cooper, Rev. Mod. Phys. **40**, 441 (1968); D. A. Outka and J. Stöhr, J. Chem. Phys. **88**, 3539 (1988).

[33] L. Halonen and T. Carrington, Jr., J. Chem. Phys. **88**, 4171 (1988).

[34] Z. F. Liu, G. M. Bancroft, and J. S. Tse (unpublished).

[35] U. Nielson, R. Haensel, and W. H. E. Schwarz, J. Chem. Phys. **61**, 3581 (1974).

[36] Derived from the results of analysis of Ref. [10].

[37] D. A. Shaw, D. Cvejanović, G. C. King, and F. H. Read, J. Phys. B **17**, 1173 (1984).

[38] L. S. Cederbaum, J. Chem. Phys. **78**, 5714 (1983).

[39] H. Nakamatsu, T. Mukoyama, and H. Adachi, J. Chem. Phys. **95**, 3167 (1991).

[40] H. Friedrich, B. Sonntag, P. Rabe, W. Butscher, and W. H. E. Schwarz, Chem. Phys. Lett. **64**, 360 (1979).

[41] L. C. Lee, X. Wang, and M. Suto, J. Chem. Phys. **86**, 4353 (1987).

[42] X. Xie, L. Schnieder, H. Wallmeier, K. H. Welge, and M. N. R. Ashfold, J. Chem. Phys. **92**, 1608 (1990), and references therein.

[43] K. Weide, V. Staemmler, and R. Schinke, J. Chem. Phys. **93**, 861 (1990); B. Heumann, R. Duren, and R. Schinke, Chem. Phys. Lett. **180**, 583 (1991).

[44] M. Braustein and R. T. Pack, J. Chem. Phys. **96**, 891 (1992).

[45] M. O. Krause and J. H. Oliver, J. Phys. Chem. Ref. Data **8**, 329 (1979).

[46] D. Thomas (private communication).

[47] A. Cesar and H. Agren (unpublished), cited in Ref. [16].